Inter-ply stitching optimisation of highly drapeable multi-ply preforms

S Chen, A Endruweit, L T Harper, N A Warrior

Polymer Composites Group, Division of Materials, Mechanics and Structures, Faculty of Engineering, The University of Nottingham, UK, NG7 2RD

Abstract

An efficient finite element model has been developed in Abaqus/Explicit to solve highly non-linear fabric forming problems, using a non-orthogonal constitutive relation and membrane elements to model bi-axial fabrics. 1D cable-spring elements have been defined to model localised inter-ply stitch-bonds, introduced to facilitate automated handling of multi-ply preforms. Forming simulation results indicate that stitch placement cannot be optimised intuitively to avoid forming defects. A genetic algorithm has been developed to optimise the stitch pattern, minimising shear deformation in multi-ply stitched preforms. The quality of the shear angle distribution has been assessed using a maximum value criterion (MAXVC) and a Weibull distribution quantile criterion (WBLQC). Both criteria are suitable for local stitch optimisation, producing acceptable solutions towards the global optimum. The convergence rate is higher for MAXVC, while WBLQC is more effective for finding a solution closer to the global optimum. The derived solutions show that optimised patterns of through-thickness stitches can improve the formability of multi-ply preforms compared with an unstitched reference case, as strain re-distribution homogenises the shear angles in each ply.

Keywords

A. Fabrics/textiles; E. Forming; E. Preform; E. Stitching

1. Introduction

For medium volume applications, composite components are frequently manufactured based on preforming of fibrous reinforcement structures, followed by impregnation with a thermoset resin. The challenge in introducing advanced preforming technologies is characterising and optimising the forming behaviour of 2D reinforcements in order to produce repeatable 3D components with acceptable quality, which is related to the level of shear deformation. In particular, wrinkling and fibre buckling are undesirable in a preformed reinforcement because of the influence on mechanical properties. Fixation of the fibrous structure through application of through-thickness stitch-bonds reduces in-mould assembly time and can aid robotic placement by enabling multi-layer stacks to be processed as one single preform. Previous research on reinforcement forming has generally addressed the simulation of components consisting of a single fabric ply [1, 2], or preforms of multiple plies with identical orientation [3, 4], where the difference in draw-in between plies and inter-ply friction is not as significant as in heterogeneous multi-ply preforms [5, 6]. However, little work has been reported on forming of complex stacking patterns or multi-ply preforms containing localised stitch-bonds. The present work seeks to understand the opportunities offered by locally stitching multiple plies together to create a single preform blank which can be formed into a complex 3D shape.

One approach for simulation of multi-ply forming is to use multi-layered finite elements (FE), where one layer of elements represents multiple fabric layers, for more efficient simulation [6]. However, this method ignores relative sliding between plies, which is one of the main forming modes for multi-ply systems. In order to account for sliding, each ply needs to be modelled independently as a separate element layer. Cheruet et al. [7] modelled forming of a Z-shaped component consisting of 10 pre-impregnated plies and found that predicted relative inter-ply sliding agreed well with experimental data. Harrison et al. [8] conducted forming simulations for two cross plies (0°/90° UD) of thermoplastic prepreg, assuming a biaxial constitutive relationship. The viscous nature of the matrix material ensured

that the main in-plane deformation mode was trellising (shear), similar to a woven material. However, when the fibres are dry, the deformation mechanism changes, and intra-ply sliding of loosely fixated yarns becomes more important, particularly for multi-ply forming of non-crimp fabrics (NCF) [9]. Experimental results show that NCFs experience high levels of slip within each layer of the bi-directional material, as the stitches provide less restraint than interweaving of warp- and weft-yarns. This phenomenon was captured in simulations by using bar elements to represent the stitch between UD plies modelled as shell elements. Good agreement was shown between numerical simulations and experimental results for forming of a hemisphere, but sliding was limited to the fibre direction, which may be an oversimplification for more complex geometries.

Investigations into the influence of stitches have been generally limited to studying intra-ply stitches in NCFs [9] or single woven plies [3], to understand how they can be used to control local yarn angles. Molnar et al. [4] investigated the influence of inter-ply stitching experimentally. Local stitch-bonds were found to affect shear deformation in the formed fabric. It was concluded that it is possible to transfer shear forces into un-sheared regions of the ply during forming. Through-thickness stitching in multi-ply preforms has been simulated in explicit finite element analyses using spot weld constraints [3, 10]. Whilst only multi-ply stacks with identical ply orientations were studied, for certain cases, redistribution of strains within the fabric through use of stitches was proven feasible to avoid wrinkling. Duhovic et al. [3] studied the force-displacement relationship for stitches in detail. It was found that stitches did not restrict the fabric shear behaviour when a strain offset was defined to account for slack in the thread during tensile loading, and was set to a value obtained from experiments. Bel et al. [11] investigated the influence of local stitch-bonds on preforming of commercial components, using beam spring elements to model the stitches in explicit FE studies.

Margossian et al. [12] found that the contribution of stitches to the in-plane mechanical properties of a ply is almost negligible compared to that of the yarns in the fabric. Assembly stitches behave as additional local inter-ply constraints, providing connecting forces to

decrease the relative local inter-ply displacement. This effect becomes much more significant for adjacent plies with different initial fibre orientations, since the relative inter-ply displacement is greater under these circumstances. Since their in-plane influence can be ignored, each through-thickness stitch can be considered in isolation (in-plane stitch path can be overlooked).

Shear deformation in the fabric plies caused by the introduction of stitch bonds may negatively affect the properties of the finished component. A mathematical algorithm is required to determine optimised stitching patterns, to minimise local fabric shear. While there is no published work on the optimisation of inter-ply stitching, several suitable approaches have been identified from other optimisation problems. For optimisation based on large numbers of non-linear FE analyses, the enumeration approach is unsuitable, as the total computation time is unfeasibly long. Also, gradient/sensitivity-based search methods are inapplicable due to the lack of explicit relationships between the stitching patterns and the shear angle distribution. On the other hand, heuristic algorithms are an effective way to solve problems with large numbers of variables, and consequently genetic algorithms (GAs) have been chosen for this work.

This paper presents a finite element model developed to study the effect of local stitch-bonds in multi-ply preforms, particularly those with multiple ply orientations. Results from a numerical study of a simple hemisphere geometry demonstrate the capability of simulating the forming behaviour of a multi-ply stack in a single operation. A genetic algorithm has been developed to determine the optimum position of local stitches, in order to improve preform quality and ultimately facilitate automated component manufacture. Two different criteria have been implemented to assess the forming outcome; the maximum value criterion (MAXVC) and the Weibull distribution quantile criterion (WBLQC). The convergence rates and optimum solutions for both criteria have been compared to understand the compromise between accuracy and computational efficiency.

2. Modelling approach

2.1 Material model for non-orthogonal bi-axial materials

The proposed material model captures the dominant factors in fabric forming, including in-plane shear, fibre elongation and inter-tow/intra-ply slipping. A macro-scale homogenisation scheme has been adopted to avoid modelling discrete tows. The effects of parameters associated with the fibre architecture (yarn spacing, cross-sectional shape, crimp etc.) are captured in the in-plane shear behaviour, which is defined by a non-linear stress-strain curve with a progressive hardening step. A hypo-elastic model [5, 13] has been adopted to capture both material and geometric non-linearity due to large displacements and large rotations of the yarns [5, 13, 14]. Elastic models are typically used for forming simulations for simplicity, even though the fabric response during deformation is not necessarily elastic. However, deformation is arrested when the forming process is complete in order to conform to permanent deformation [15].

2.1.1 Implementation of material model

The material model is implemented in a user-defined subroutine in Abaqus/Explicit. A non-orthogonal fibre coordinate system, where the axes coincide with the current orientations of yarns at any material point, has been used. The non-orthogonal constitutive relation captures anisotropic behaviour of biaxial composite materials under large shear deformation more accurately than an orthogonal model [16, 17]. A VFABRIC subroutine has been developed to define the mechanical constitutive relations of woven fabrics. The VFABRIC routine is valid for materials that exhibit two structural directions, which may not remain orthogonal following deformation.

The non-orthogonal material model is summarised in Fig. 1. The in-plane engineering strains at the beginning of each time increment in the explicit time integration scheme ($\varepsilon_{f_1}^{old}$, $\varepsilon_{f_2}^{old}$, $\gamma_{f_1 f_2}^{old}$ i.e. $[\varepsilon]_{f_1 f_2}^{old}$) and the corresponding strain increments ($d\varepsilon_{f_1}$, , $d\varepsilon_{f_2}$, $d\gamma_{12}$ i.e. $[d\varepsilon]_{f_1 f_2}$) are calculated internally. The raw material data are transformed to the current non-

orthogonal fibre coordinate system. For each fibre direction in the non-orthogonal system, material properties ($[\mathrm{C}]_{f_1}^{ort}$, $[\mathrm{C}]_{f_2}^{ort}$) are defined in an orthogonal system, where one base vector is parallel to the fibre direction. For the fabric forming process, the shear deformation can be large, and the two yarn orientations may no longer be perpendicular to each other during forming. Material properties are transformed into the non-orthogonal fibre coordinate system ($[\mathrm{C}]_{f_1 f_2}^{non-ort}$) using the current coordinate transformation matrix, $[\mathrm{Q}]$. Finally, the initial stress tensor ($[\sigma]_{f_1 f_2}^{old}$) can be updated to be $[\sigma]_{f_1 f_2}^{new}$ by superimposing it with the stress increment tensor ($[d]_{f_1 f_2}$), which is calculated from the current constitutive matrix in the non-orthogonal fibre coordinate system. This is subsequently returned to Abaqus/Explicit for further processing.

Although material properties along the fibre directions (such as E_{11}) can be applied directly in VFABRIC, other properties (such as E_{12}) need to be transformed into the non-orthogonal fibre coordinate system (i.e. the system defined by the warp-fibre vector $\underline{\mathrm{f}}_1$, the weft-fibre vector $\underline{\mathrm{f}}_2$ and the out-of-plane vector $\underline{\mathrm{f}}_3$) using the current coordinate transformation matrix. Only very minor modifications are required in VFABRIC to establish a non-orthogonal constitutive matrix compared with the more generalised VUMAT approach in Abaqus/Explicit. Implementing a VFABRIC routine therefore reduces the number of tensor operations and results in a more computationally efficient model.

2.1.2 Material model validation

Numerical tests have been performed to verify that the constitutive relation used in the current VFABRIC subroutine is correct for bi-axial fabrics, using experimental and numerical data from the International Forming Benchmark study [18]. The choice of material parameters is consistent with published data [5, 13, 19, 20] for a balanced plain weave glass/polypropylene commingled fabric. The value of Young's modulus was taken to be

constant (35.4 GPa) in each fibre direction, ignoring any initial non-linearity in the stress-strain curve due to fibre crimp. Including the influence of fibre crimp in the material model was found to have an insignificant effect on the forming behaviour of a woven glass fabric in hemisphere forming simulations by Boisse et al [1]. The shear modulus was described by the polynomial:

$$G_{12} = (6.7135|\gamma_{12}|^4 - 9.8228|\gamma_{12}|^3 + 6.3822|\gamma_{12}|^2 - 1.5928|\gamma_{12}| + 0.1948)\ \text{MPa} \quad \text{Eqn. 1}$$

where γ_{12} is the in-plane shear angle in radians.

Each ply was discretised into 4096 square membrane elements (Abaqus/Explicit element type M3D4R). All parts of the tooling were considered to be rigid bodies. A penalty contact algorithm was used to define the behaviour at all interfaces. An isotropic Coulomb friction model was adopted for both the tooling-material and material-material contacts with a constant coefficient of 0.2. Displacement boundary conditions were applied to the punch and a force of 100 N was applied to the blank holder to control blank slippage. Two material configurations were studied during the validation stage; forming of a single 0°/90° ply and a single ±45° ply.

The run time of the model is important for successful implementation of the stich optimisation, as large numbers of iterations need to be run to determine the optimum pattern. Both mass scaling (MS) and time scaling (TS) have been evaluated in this study to reduce CPU time. Fig. 2 indicates that there is a very strong correlation between experimental forming results from the literature [5, 13, 20, 21] and numerical forming results based on the VFABRIC model developed here, and that TS or MS do not compromise the validity of the simulation results. Both shear angle distribution and material draw-in are very closely matched when adopting MS or TS. The local shear angle has been checked at 10 discrete points (see

Table 1) and compared quantitatively against experimental data [5, 13]. The peak shear angles differ by about 3 % (1.26°) between the MS and TS models.

The element edges in the mesh for each ply are aligned with the geometry axes, rather than with the fibre orientations, which facilitates definition and implementation of inter-ply stitches in the numerical model. A sensitivity analysis has been performed to assess the potential issue of finite element shear locking for cases where the material directions are not aligned with the element edges, which is discussed in the literature [22, 23]. Simulation results for local shear angle distributions in 0°/90° and ±45° fabric plies at different mesh orientations are plotted in Fig. 3. The shear angle distributions for the 0°/90° ply appear to be insensitive to the mesh orientation, with maximum shear angles of 42.54° (aligned) vs 43.54° (misaligned) respectively. For the ±45° ply, differences in local shear angle distributions for different mesh alignment are more significant than for the 0°/90° case, but the difference between maximum shear angles, 44.89° (aligned) and 43.67° (misaligned), is still small. Since global ply deformation patterns appear to be unaffected, and hence no significant effect on the outcome of the stitch optimisation is anticipated, a slight reduction in accuracy of results for plies with misalignment between material orientations and mesh orientations is considered acceptable here.

2.2 Inter-ply stitch model

Assembly stitches have been modelled as inter-ply connections by constraining coincident nodes using a user-defined 1D cable-spring element in Abaqus/Explicit, as shown in Fig. 4. Both ends of each stitch element have unconstrained rotational degrees of freedom, and the compression modulus is set to zero, hence providing tensile stiffness only. A degree of ‘slack’ is built into the model by enabling the stitch elements to extend under zero tensile load (see Fig. 5). The behaviour of the stitch is defined by the tensile stiffness along the axial direction and the initial slack length. The presence of the stitch does not influence the friction

between the fabric plies, since the spring element represents a constraint of nodal mobility without physical surface properties.

The stitch constrains nodal displacement, as shown in Fig. 4. The magnitude of the reaction force is equal to the axial stitch force. For an arbitrary inter-ply stitch element connecting nodes i and j, the relative displacement Δl_{ij} can be calculated as

$$\Delta l_{ij} = \left|\vec{l}_{i'j'}\right| - \left|\vec{l}_{ij}\right| \quad \text{Eqn. 2}$$

$$\vec{l}_{i'j'} = \vec{l}_{oj'} - \vec{l}_{oi'} = (x_{j'}, y_{j'}, z_{j'}) - (x_{i'}, y_{i'}, z_{i'}) \quad \text{Eqn. 3}$$

$$\vec{l}_{ij} = \vec{l}_{oj} - \vec{l}_{oi} = (x_j, y_j, z_j) - (x_i, y_i, z_i) \quad \text{Eqn. 4}$$

where (x_i, y_i, z_i) and (x_j, y_j, z_j) are the initial nodal positions of a stitch element, while $(x_{j'}, y_{j'}, z_{j'})$ and $(x_{i'}, y_{i'}, z_{i'})$ are the current nodal positions of the same stitch element. All of these coordinates are calculated by Abaqus/Explicit at each time increment.

As shown in Fig. 5, the axial stiffness of a stitch (i.e. k^{st}) is defined as

$$k^{st} = \begin{cases} 0 & , \quad \Delta l_{ij} \leq \Delta l_c \\ k_{ten}^{st} & , \quad \Delta l_{ij} > \Delta l_c \end{cases} \quad \text{Eqn. 5}$$

where the superscript "*st*" denotes properties associated with the stitch element, Δl_c is the critical relative displacement to identify whether the stitch element is slack or stretched, and k_{ten}^{st} is the tensile stiffness along the axial direction. These parameters can be obtained from material testing [3]. Values of $k_{ten}^{st} = 32.55\ \mathrm{kN/m}$ and $\Delta l_c = 0.57\ \mathrm{mm}$ [3] have been used throughout this study.

Hence, the axial force for each stitch element (i.e. F_{ij}^{st}) can be calculated as

$$F_{ij}^{st} = k^{st} \cdot \Delta l_{ij} \quad \text{Eqn. 6}$$

The stitch force is updated in each time increment by invoking the above 1D user-defined stitch element.

An example of a stitched preform stack is shown in Fig. 6 for a hemisphere geometry. The preform consists of four plies with dimensions 320 mm×320 mm and a thickness of 1 mm

in a $[(0°/90°) / \pm 45°]_s$ configuration. The hemisphere has a diameter of 100 mm, and the formed height is 50 mm. Stitch bonds have been applied at every node along the two diagonals from corner to corner.

The numerically calculated maximum shear angle for this case (78.29°) is significantly higher than the values for the example in Fig. 2, resulting in visible wrinkles on the formed hemispherical surface. This maximum shear angle exceeds the shear locking angle of the fabric (approximately 45° [19]). Unrealistically high values like this can occur as a consequence of the polynomial fit to the high shear modulus region of the experimental shear data [17]. The stitch paths go through the centre of the highest sheared regions in the 0°/90° plies, which results in the shear deformation being distributed more globally than in the unstitched case, since the mobility of the fibres along the diagonals is restricted. This can be seen clearly in Fig. 7, which shows the local shear angles plotted along a diagonal path from the centre of the hemisphere to the top-right hand corner. Large deformations in the ±45° plies occur due to them being directly coupled to the 0°/90° plies. These results highlight the consequence of choosing a poor stitch pattern and emphasise the importance of developing a stitch optimisation routine to reduce excessive shear deformation.

3. Methodology of stitching optimisation

The stitching optimisation is implemented using Matlab, as shown in Fig. 8. For each loop or “generation” in the GA, a group of stitching patterns called “individuals” is generated, and Abaqus/Explicit input files are produced. Abaqus/Explicit simulations are employed to determine the shear angle distribution for each individual, which is then returned to Matlab. For the returned shear angle data, the corresponding fitness value is determined individually to check for convergence. This loop repeats until the optimum is achieved.

3.1 Implementation of genetic algorithm

A binary encoding method is applied to formulate each individual stitching pattern for the optimisation algorithm. Each stitching pattern represents a binomial-status series, which can be described numerically by the encoding scheme in Fig. 9. Each bit in the binary code represents one potential stitching position and its value corresponds to a "stitched" or "unstitched" status. By using this encoding scheme, the physical problem can be converted into a mathematical problem to perform a series of GA manipulations to heuristically search for the optimum stitch pattern.

The stitching optimisation problem can be written as:

$$\text{Minimise: } f\{p_1, p_2, \cdots, p_n;\ \gamma_{12}(x, y, z)\} \quad \text{Eqn. 7}$$

$$\text{subject to: } p_i = \begin{cases} 1, & \text{stitched} \\ 0, & \text{unstitched} \end{cases} \quad (i = 1,2, \cdots, n) \quad \text{Eqn. 8}$$

$$\gamma_{12}(x, y, z) \in [0°, 90°] \quad \text{Eqn. 9}$$

$$(x, y, z) \in \Omega_M \quad \text{Eqn. 10}$$

where, $f\{\cdot\}$ is the fitness function of the stitching optimisation in GA to describe the selection criterion, which is employed to assess the distribution of shear angles in the material field. p_i $(i = 1,2, \cdots, n)$ is the i^{th} optimisation variable, which denotes the stitching status at the i^{th} potential stitching position. n is the total number of potential stitching positions.

3.2 Fitness function

The fitness function is used to assess how well each individual stitch pattern is adapted to the assessment criteria. Its value reflects the relative distance from the optimum solution, where a smaller value is preferential. During stitching optimisation, the aim is to optimise the shear angle distribution in the spatial material field. However, the shear angle is a field variable which it is too difficult to optimise directly. Hence, an appropriate fitness function is defined using a reduced mathematical expression, which is easier to manipulate numerically.

Appropriate selection of the fitness function is important, as it dominates the convergence rate of optimisation and the accuracy of the optimum solution.

At the material level, characterisation of in-plane shear is assessed by measuring the non-linear mechanical response of the material during shear loading. A limit is often imposed on the level of deformation, in the form of a "locking angle" [2], which is the point at which tows are no longer able to rotate freely. The locking angle represents the maximum level of shear deformation that can be achieved before material wrinkling/buckling occurs, which is undesirable in a preformed reinforcement because of the influence on mechanical properties [19]. The objective is therefore to keep all local shear angles below the locking angle. Since the value of shear angle is limited by

$$|\gamma_{12}(\mathrm{x},\mathrm{y},\mathrm{z})| \in \left[0, \max_{(\mathrm{x},\mathrm{y},\mathrm{z})\in\Omega_{\mathrm{M}}}\{|\gamma_{12}(\mathrm{x},\mathrm{y},\mathrm{z})|\}\right] \quad \text{Eqn. 11}$$

the optimisation objective can be reduced to minimise the maximum shear angle, referred to in this work as the maximum value criterion (MAXVC). The maximum can be derived from the finite element approximation for $|\gamma_{12}(\mathrm{x},\mathrm{y},\mathrm{z})|$. Thus,

$$f_{MAXVC}\{p_1, p_2, \cdots, p_n;\ \gamma_{12}(x,y,z)\} = \max_{(x,y,z)\in\Omega_M}\{|\gamma_{12}(x,y,z)|\} \approx \max_{\mathrm{i}=1,2,\cdots,\mathrm{N}}\{\gamma_{\mathrm{i}}\} \quad \text{Eqn. 12}$$

where $f_{MAXVC}\{\cdot\}$ denotes the fitness function using MAXVC; Ω_M is the spatial material region; $\gamma_{12}(x,y,z)$ is the continuous shear angle distribution in the material region Ω_M; N is the total number of material points; $|\cdot|$ is the absolute value of the variable; $\gamma_{\mathrm{i}} = |\gamma_{12}(x_i, y_i, z_i)|$ is the absolute value of the shear angle at the i^{th} material point (x_i, y_i, z_i). Since the stitching pattern determines the obtained shear angle distribution, the value of f_{MAXVC} is used for quantitative assessment of the fitness of the corresponding stitching pattern.

Although MAXVC is suitable for assessing the behaviour for most conditions, it can be somewhat conservative for achieving fast convergence. Additionally, the maximum shear angle only represents an upper bound and may not be representative of the overall distribution, resulting in an unfavourable stitch placement decision. For example, it may not be sensible to use this criterion when only a small number of elements exhibit extremely large

shear angles, as these may be classed as outliers, and consequently the global shear angle distribution will be unaffected by the optimisation procedure [24]. Hence, a more global criterion is employed to summarise the shear angle data and a corresponding statistical criterion is proposed to assess the fitness of the stitching pattern. Since Extreme Value Theory suggests that the Weibull distribution is suitable for modelling mechanical failure phenomena [25, 26], a two-parameter Weibull distribution is analogously employed here to characterise the stochastic behaviour of the shear angle distribution. The cumulative distribution function (CDF), $F(\gamma;\eta,\beta)$, is expressed as

$$F(\gamma;\eta,\beta) = 1 - e^{-\left(\frac{\gamma}{\eta}\right)^{\beta}}, \gamma \in [0,+\infty) \quad \text{Eqn. 13}$$

where η ($\eta > 0$) is the scale parameter and β ($\beta > 0$) is the shape parameter for the two-parameter Weibull distribution. Thus, their corresponding estimators, $\hat{\eta}$ and $\hat{\beta}$, can be determined by combining the following two equations obtained from the maximum likelihood method

$$\hat{\eta} = \left[\left(\frac{1}{N}\right)\sum_{i=1}^{N}\gamma_i^{\hat{\beta}}\right]^{\frac{1}{\hat{\beta}}} \quad \text{Eqn. 14}$$

$$\hat{\beta} = \frac{N}{\frac{1}{\hat{\beta}}\cdot\sum_{i=1}^{N}\left(\gamma_i^{\hat{\beta}}\cdot\ln\gamma_i\right) - \sum_{i=1}^{N}(\ln\gamma_i)} \quad \text{Eqn. 15}$$

where $\hat{\eta} > 0$ and $\hat{\beta} > 0$. The unknown parameters $\hat{\eta}$ and $\hat{\beta}$ are calculated by solving Eqn. 14 and Eqn. 15 numerically; based on $\gamma_1, \gamma_2, \cdots, \gamma_N$, which are obtained from finite element analysis. If $\gamma_{1-\alpha}$ is the upper α quantile of the distribution, i.e. the probability to find a shear angle with a value greater than $\gamma_{1-\alpha}$ is α, then

$$\mathrm{F}(\gamma_{1-\alpha}) = 1 - \alpha = 1 - e^{-\left(\frac{\gamma_{1-\alpha}}{\hat{\eta}}\right)^{\hat{\beta}}} \quad \text{Eqn. 16}$$

is the probability to find a shear angle smaller than $\gamma_{1-\alpha}$. When α has a small enough value (typically 0.05), and the distribution parameters have been estimated, the equation can be

solved for $\gamma_{1-\alpha}$. This is considered to be the extreme value (i.e. the maximum shear angle) with a probability of $(1-\alpha)$ [25].

Instead of using the maximum shear angle from all material points, the statistical extreme value is employed to represent the fitness score for each stitching pattern. The lower this value becomes, the better the stitching pattern. Hence, the fitness function using the Weibull distribution quantile criterion (WBLQC) can be written as

$$f_{\mathrm{WBLQC}}\{p_1, p_2, \cdots, p_n;\ \gamma_{12}(x,y,z)\} = \gamma_{1-\alpha} = \hat{\eta} \cdot \left(\ln \frac{1}{1-\alpha}\right)^{\frac{1}{\hat{\beta}}} \quad \text{Eqn. 17}$$

3.3 Adaptive programming strategy

Due to the non-analytical relation between stitching pattern and shear angle distribution, shear angle data must be collected for every individual stitching pattern from FE analyses. Although the run time for each simulation has been reduced by mass scaling, processing a large number of FE jobs in series (Fig. 10(a)) is not an efficient way to conduct the optimisation, because of considerable idling time of computational resources. It is also impractical to utilise a parallel algorithm to submit the jobs simultaneously (Fig. 10(b)), since only a limited number of jobs can be submitted each time, due to typical constraints on the number of software licenses available and computing hardware. Thus, an adaptive hybrid algorithm has been developed for running the stitch optimisation as shown in Fig. 10(c). It can manage and balance the computational resources and task allocation effectively, according to real-time feedback information.

4. Results and discussion

Stitching patterns were optimised for a hemisphere model with a diameter of $100\ mm$. The model consisted of a matched punch and die, with a planar blank holder applying normal pressure to the material to maintain tension in the tows throughout the forming process. The blank consisted of 4 plies of the same balanced woven fabric with the same properties as in

Section 2.1.2, using a symmetric layup $[(0°/90°) / \pm 45°]_s$. The plies were numbered in order from bottom to top as 1st ply to 4th ply.

The mechanical properties of stitches defined in Section 2.2 were assigned to every stitch element in each finite element model where applicable. In total, 81 potential positions, spaced at 40 mm intervals on a regular square grid, were considered as stitching variables. The population size was 100 in each generation and the tolerance for the fitness function was 0.05°. The crossover and mutation coefficients were 0.80 and 0.20 respectively.

To compare the natural selection criteria, both MAXVC and WBLQC were employed to execute the optimisation. Several generations have been selected to illustrate the optimisation evolutions using different fitness functions in Fig. 11. Each generation represents a summary of 100 individual stitch patterns, where the dots represent the locations for clusters of stitches, rather than individual stitches. The choice of the individuals in the initial population may influence the convergence speed, but not the final stitch pattern. The initial population of 100 patterns for the zeroth generation was generated randomly, which then evolve into subsequent generations according to the genetic algorithm. The number of individuals is chosen to be greater than the number of variables (81) to ensure a diverse population. The low tolerance for the fitness function ensures that the optimisation procedure is not terminated prior to achieving the optimum.

The frequencies for occurrence of each of the 81 stitch positions were equally represented in the zeroth generations in Fig. 11, as indicated by a relatively uniform red level for each dot. The shade of red changes as the stitch patterns evolve for each subsequent generation, where a darker red (tending towards black) represents a higher frequency for that stitch position and a lighter shade of red (tending towards white) represents a lower frequency. As the fitness function converges, all dots appear black, which indicates that all 100 stitch patterns for that generation are the same.

Fig. 11 indicates that: (1) both natural selection criteria converge to produce respective optimum solutions, even though their searching directions are different; (2) the final

converged stitch positions are similar for both selection criteria. The basic patterns resemble a quadrilateral with a cross running through the centre and several additional stitches around the edges. However, their dimensions are different; (3) the convergence speed is faster for MAXVC (generation 28) than for WBLQC (generation 35). Whilst the shear angle distributions for the unstitched case are totally symmetrical, there are no symmetry conditions imposed during the optimisation process. Therefore the optimum stitch patterns are not always symmetrical, leading to asymmetric shear angle distributions.

The unstitched case was taken as a reference case to evaluate the quality of the stitch optimisation. Fig. 12 shows that the maximum shear angle of the optimum case using MAXVC ($42.51°$) is slightly smaller than for the unstitched case ($43.99°$). However, the maximum shear angle from the WBLQC criteria ($56.54°$) is significantly higher than the maximum of the unstitched case. For this particular scenario, the shear angles of the 4 corner elements are extremely large and are far from the global average. Thus, they can be considered to be outliers. These severely sheared areas are small relative to the whole material field and are located at the perimeter of the blank away from the final formed surface. They will not influence the quality of the final component, but this outcome highlights the relevance of the statistical criterion.

The global distribution of shear angles produced from the two criteria is almost identical as shown in Fig. 12. Hence, both criteria appear to produce sensible solutions. Severely sheared regions (i.e. red) only occur in the $0°/90°$ plies (i.e. 1st and 4th plies), whilst the maximum shear angle for the $\pm 45°$ plies (i.e. 2nd and 3rd plies) is smaller. This phenomenon is captured by both criteria.

The shear angle distributions have been plotted on the undeformed blank shape and normalised with respect to the unstitched configuration to make comparisons easier, as illustrated in Fig. 13. The blue regions represent a reduction in shear angle compared with the unstitched case and red indicates an increase. For the $0°/90°$ plies (i.e. 1st and 4th plies), which were shown to have the highest sheared regions in Fig. 12, the blue areas are larger

and darker for the WBLQC case in Fig. 13(a) than for the MAXVC case in Fig. 13(b). Hence, the optimum stitch patterns that result from the WBLQC effectively homogenise the global shear angle distribution more than the MAXVC, as expected. Reduction in size and intensity of the blue regions is not so considerable for the $\pm 45°$ plies (i.e. 2nd and 3rd plies) according to Fig. 13.

There are also regions of increasing shear angle for both converged solutions, since load paths have been changed by placing localised stitches. These regions experience more deformation than in the unstitched case due to strain re-distribution through localised stitches, which flatten the shear profile in high deformation regions. The influence of these local increases depends on the affected area as well as its final absolute shear angle. If these increases occur on the formed surface of the final component then these effects can be considered to be negative. However, most of the darker red regions are concentrated around the edges of the blank and are therefore not critical in this case. Fig. 13indicates that the increasing shear angle regions (red regions) do not reduce the overall quality of the preform, as the global shear angle is generally less than 30°, with only small discrete regions approaching 50°. Stitch patterns produced by WBLQC yield shear angle distributions closer to the unstitched benchmark solution and can provide better quality formed parts. However, the cost of using WBLQC is higher, taking more computational time to converge than MAXVC.

The optimisation procedure has successfully homogenised both the local and global shear angle distributions, using both criteria. However, it is important to avoid introducing additional defects when minimising the local shear angle. The compressive strains in the fibre direction (1-direction) have been plotted in Fig. 14 to understand the likelihood of bundle wrinkling, as reported by Long et al. [27]. (Strain distributions in 2-direction are similar). In general, there is a reduction in the magnitude of the compressive strains for the two optimised cases, with the WBLQC case indicating the lowest risk of bundle wrinkling. This provides further confidence in the optimisation results, but is only a qualitative assessment that requires further experimental validation.

5. Conclusions

A finite element model has been developed to solve complex forming problems consisting of multi-ply preforms containing localised stitch-bonds. A non-orthogonal constitutive relation has been defined for bi-axial materials with large deformation, using a user-defined VFABRIC model in Abaqus/Explicit. Assembly stitches have been modelled using user-defined 1D cable-spring elements. A simulation was performed for a balanced 4 ply preform with stitches applied in a diagonal configuration. Results indicated that the local maximum shear angle was significantly higher than in the unstitched case, and local stitch-bonds influence the global shear angle distribution rather than having just a localised effect. It was concluded that placing stitch bonds is not an intuitive process and this highlighted the need for a stitch optimisation routine.

An optimisation methodology has been developed for placing local inter-ply stitches on multi-ply preforms, by coupling finite element analysis with a genetic algorithm. A binary encoding scheme has been employed and two different criteria have been proposed to assess the quality of the shear angle distribution for the optimised solution; the maximum value criterion (MAXVC) and the Weibull distribution quantile criterion (WBLQC). An adaptive hybrid processing strategy was designed to accelerate the optimisation by managing computational resources and task allocation efficiently.

Both MAXVC and WBLQC were found to be suitable criteria for local stitch optimisation, producing acceptable solutions towards the global optimum. The convergence speed is higher when adopting MAXVC compared with WBLQC, but WBLQC is more effective for finding a solution closer to the global optimum by eliminating the influence of outliers. The choice of criterion is therefore a compromise between optimisation quality and computational cost. According to the optimisation results, it can be concluded that using optimised patterns of through-thickness stitches can improve the formability of a multi-ply preform compared with

an unstitched benchmark. Load paths are changed globally due to strain re-distribution through the localised stitches, which results in a more uniform shear angle distribution.

Acknowledgements

This work was partially funded by the Engineering and Physical Sciences Research Council [grant number: EP/IO33513/1], through the "*EPSRC Centre for Innovative Manufacturing in Composites*"

References

[1] Boisse, P., M. Borr, K. Buet, and A. Cherouat, *Finite element simulations of textile composite forming including the biaxial fabric behaviour.* Composites Part B: Engineering, 1997. 28(4): p. 453-464.
[2] Long, A.C., *Design and manufacture of textile composites*. 2005: CRC press.pp
[3] Duhovic, M., P. Mitschang, and D. Bhattacharyya, *Modelling approach for the prediction of stitch influence during woven fabric draping.* Composites Part A: Applied Science and Manufacturing, 2011. 42(8): p. 968-978.
[4] Molnar, P., A. Ogale, R. Lahr, and P. Mitschang, *Influence of drapability by using stitching technology to reduce fabric deformation and shear during thermoforming.* Composites Science and Technology, 2007. 67(15): p. 3386-3393.
[5] Khan, M.A., *Numerical and experimental forming analyses of textile composite reiforcements based on a hypoelastic behaviour*. 2009.
[6] Ten Thije, R. and R. Akkerman, *A multi-layer triangular membrane finite element for the forming simulation of laminated composites.* Composites Part A: Applied Science and Manufacturing, 2009. 40(6): p. 739-753.
[7] Cheruet, A., D. Soulat, P. Boisse, E. Soccard, and S.-L. Poec, *Analysis of the interply porosities in thermoplastic composites forming processes.* International journal of forming processes, 2002. 5: p. 247-258.
[8] Harrison, P., R. Gomes, and N. Curado-Correia, *Press forming a 0/90 cross-ply advanced thermoplastic composite using the double-dome benchmark geometry.* Composites Part A: Applied Science and Manufacturing, 2013. 54: p. 56-69.
[9] Bel, S., N. Hamila, P. Boisse, and F. Dumont, *Finite element model for ncf composite reinforcement preforming: Importance of inter-ply sliding.* Composites Part A: Applied Science and Manufacturing, 2012. 43(12): p. 2269-2277.
[10] Sidhu, R., R. Averill, M. Riaz, and F. Pourboghrat, *Finite element analysis of textile composite preform stamping.* Composite structures, 2001. 52(3): p. 483-497.
[11] Bel, S., A. Margossian, D. Leutz, U. Beier, R. Hinterhoelzl, and K. Drechsler. *Validation of local stitching simulation for stitched ncf ply stacks*. in *The 19th International Conference on Composite Materials* 2013. pp 7070-7077
[12] Margossian, A., S. Bel, J. Balvers, D. Leutz, R. Freitas, and R. Hinterhoelzl, *Finite element forming simulation of locally stitched non-crimp fabrics.* Composites Part A: Applied Science and Manufacturing, 2014. 61: p. 152-162.
[13] Khan, M.A., T. Mabrouki, E. Vidal-Salle, and P. Boisse, *Numerical and experimental analyses of woven composite reinforcement forming using a hypoelastic behaviour. Application to the double dome benchmark.* Journal of materials processing technology, 2010. 210(2): p. 378-388.
[14] Boisse, P., *Finite element analysis of composite forming*, in *Composite forming technologies*, A. Long, Editor. 2007.
[15] Lim, T.-C. and S. Ramakrishna, *Modelling of composite sheet forming: A review.* Composites Part A: Applied Science and Manufacturing, 2002. 33(4): p. 515-537.
[16] Peng, X. and J. Cao, *A dual homogenization and finite element approach for material characterization of textile composites.* Composites Part B: Engineering, 2002. 33(1): p. 45-56.
[17] Peng, X. and J. Cao, *A continuum mechanics-based non-orthogonal constitutive model for woven composite fabrics.* Composites part A: Applied Science and manufacturing, 2005. 36(6): p. 859-874.
[18] Cao, J. *Woven composites benchmark forum, http://www.Wovencomposites.Org*. Accessed September 2013.

[19] Cao, J., R. Akkerman, P. Boisse, J. Chen, H. Cheng, E. De Graaf, J. Gorczyca, P. Harrison, G. Hivet, and J. Launay, *Characterization of mechanical behavior of woven fabrics: Experimental methods and benchmark results.* Composites Part A: Applied Science and Manufacturing, 2008. 39(6): p. 1037-1053.
[20] Peng, X. and Z.U. Rehman, *Textile composite double dome stamping simulation using a non-orthogonal constitutive model.* Composites Science and Technology, 2011. 71(8): p. 1075-1081.
[21] Boisse, P., Y. Aimène, A. Dogui, S. Dridi, S. Gatouillat, N. Hamila, M.A. Khan, T. Mabrouki, F. Morestin, and E. Vidal-Sallé, *Hypoelastic, hyperelastic, discrete and semi-discrete approaches for textile composite reinforcement forming.* International journal of material forming, 2010. 3(2): p. 1229-1240.
[22] Yu, X., B. Cartwright, D. McGuckin, L. Ye, and Y.-W. Mai, *Intra-ply shear locking in finite element analyses of woven fabric forming processes.* Composites Part A: Applied Science and Manufacturing, 2006. 37(5): p. 790-803.
[23] Ten Thije, R. and R. Akkerman, *Solutions to intra-ply shear locking in finite element analyses of fibre reinforced materials.* Composites Part A: Applied Science and Manufacturing, 2008. 39(7): p. 1167-1176.
[24] Rice, J., *Mathematical statistics and data analysis*. 2006: Cengage Learning.pp
[25] Gumbel, E.J., *Statistics of extremes*. 2012: Courier Dover Publications.pp
[26] Forbes, C., M. Evans, N. Hastings, and B. Peacock, *Statistical distributions*. 2011: John Wiley & Sons.pp
[27] Long, A., A.A. Skordos, P. Harrison, M. Clifford, and M.P. Sutcliffe. *Optimisation of sheet forming for textile composites using variable peripheral pressure*. in *SAMPE*. 2006. Paris, France. pp

6. Tables and Figures

Table 1: Comparison of shear angle data from Abaqus/Explicit VFABRIC model using time-scaling (TS) and mass-scaling (MS) against experimental results from literature [5, 13]; left: plain weave fabric at 0°/90°; right: plain weave fabric at ±45°.

0°/90° Plain Weave Fabric						±45° Plain Weave Fabric					
ID	Coord. (mm)		Shear Angle (deg.)			ID	Coord. (mm)		Shear Angle (deg.)		
	Def. X	Def. Y	Exp.	Num. (TS)	Num. (MS)		Def. X	Def. Y	Exp.	Num. (TS)	Num. (MS)
1	19	209	7.84	7.33	7.69	1	1	169	42.16	42.36	42.75
2	29	194	14.48	14.55	14.25	2	25	168	23.61	22.17	23.05
3	38	177	22.61	21.50	21.63	3	43	168	9.67	9.78	10.59
4	49	161	33.66	34.22	32.89	4	57	168	0.00	0.42	3.13
5	58	147	38.94	39.28	38.91	5	56	141	8.87	8.52	5.96
6	67	132	26.53	24.22	26.42	6	56	106	14.82	16.01	16.00
7	77	116	16.62	16.05	15.46	7	56	69	22.82	20.34	21.93
8	86	101	3.21	3.76	3.31	8	78	66	21.79	23.12	20.53
9	95	86	7.06	7.96	7.77	9	99	67	17.83	17.79	17.33
10	105	69	0.00	1.08	1.64	10	118	66	7.77	6.06	8.56
Avg. Abs. Error $\frac{1}{N}\sum\left\|\gamma_{12}^{num}-\gamma_{12}^{exp}\right\|$				0.80°	0.59°	Avg. Abs. Error $\frac{1}{N}\sum\left\|\gamma_{12}^{num}-\gamma_{12}^{exp}\right\|$				0.93°	1.28°
CPU Time				419 sec	77 sec	CPU Time				386.9 sec	93.4 sec

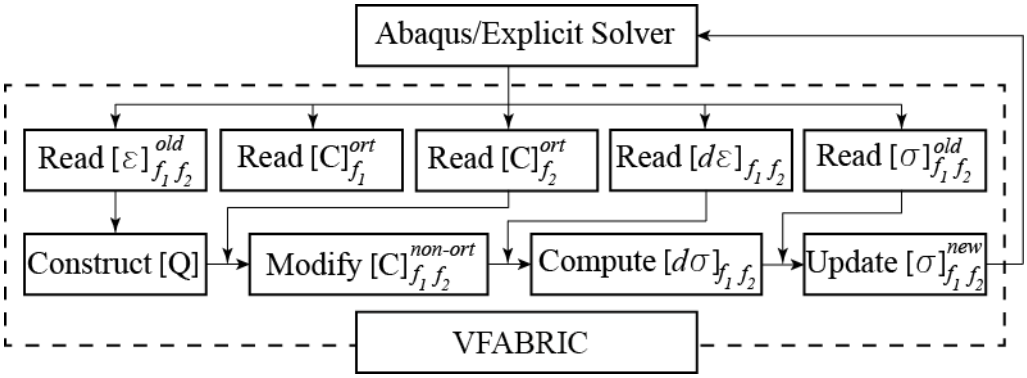

Fig. 1: Flow chart of user-defined VFABRIC material model.

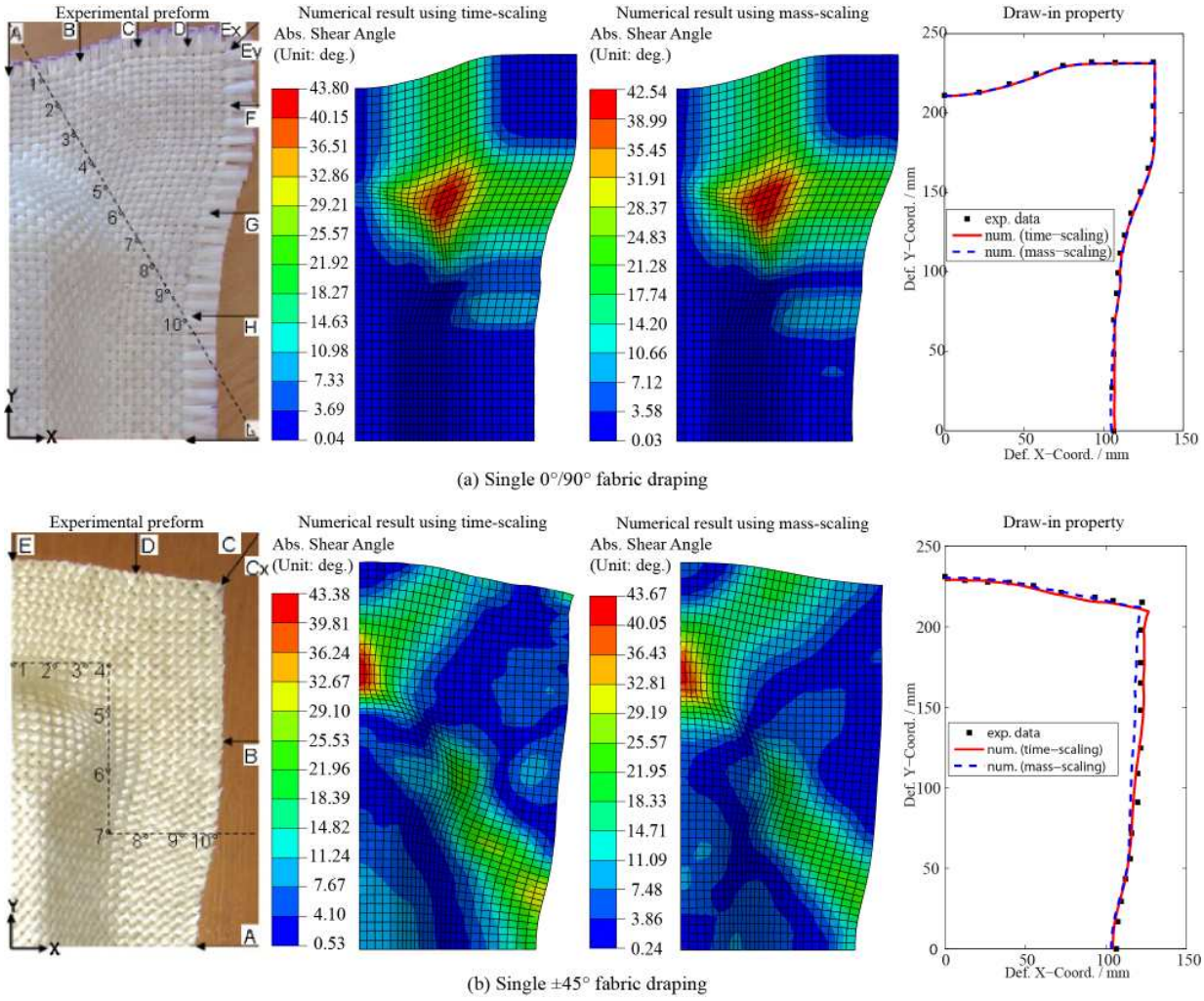

Fig. 2: Comparison of Abaqus/Explicit VFABRIC model using time-scaling and mass-scaling against experimental results from literature [5, 13]; (a) plain weave fabric at 0°/90°; (b) plain weave fabric at ±45°.

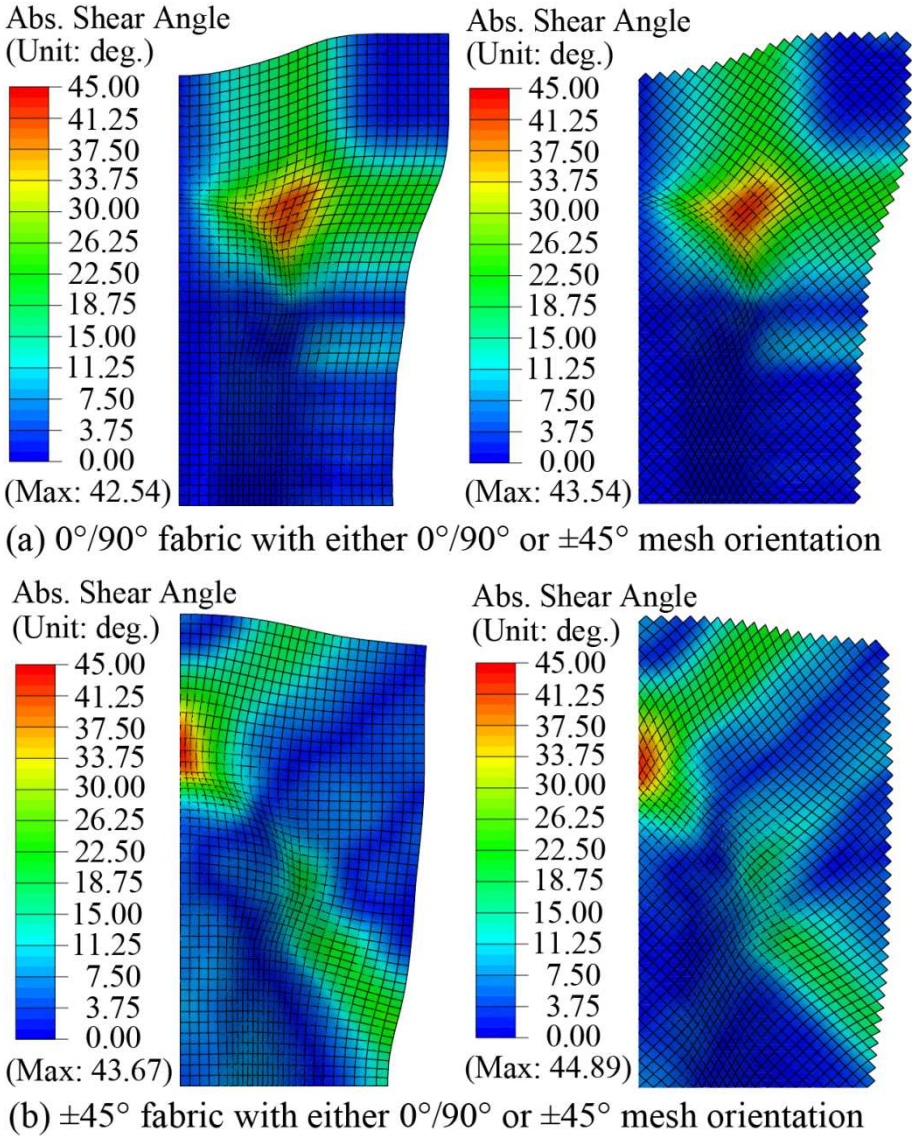

Fig. 3: The effect of mesh orientation relative to material orientations on the shear angle distribution for both 0°/90° and ±45° plies.

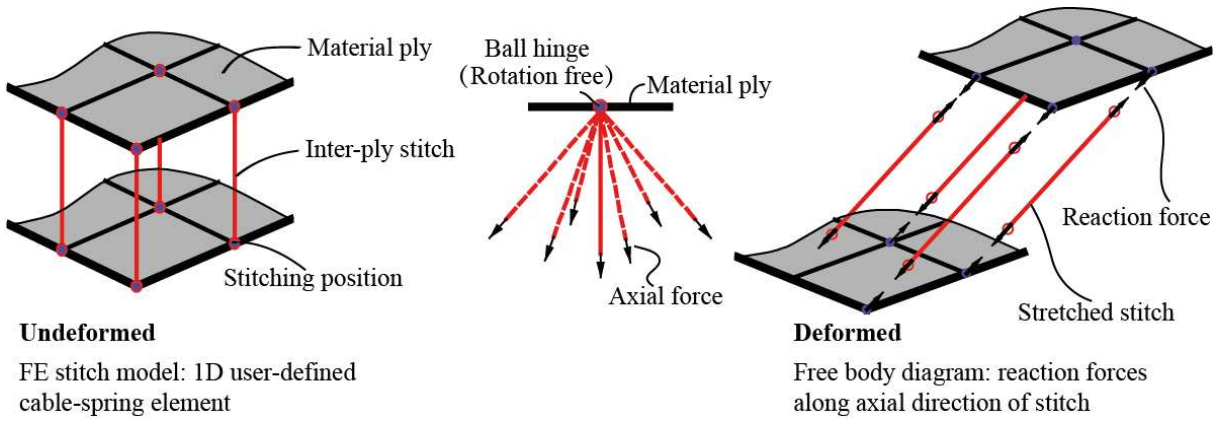

Fig. 4: Inter-ply stitch model defined in Abaqus/Explicit using 1D user-defined cable-spring element.

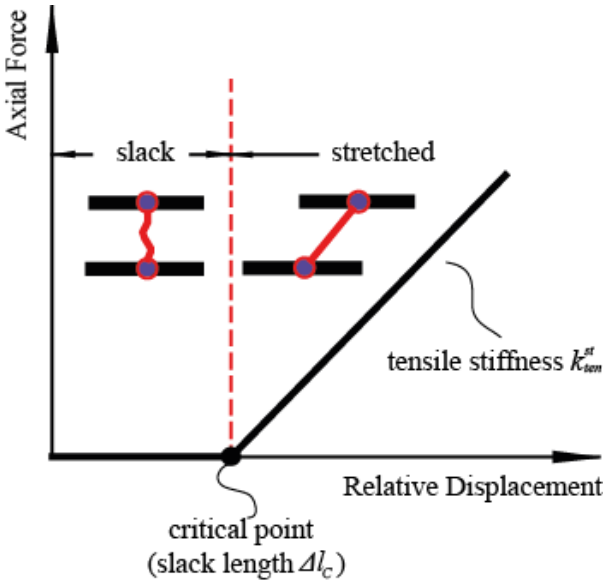

Fig. 5: Definition of axial behaviour for stitch element.

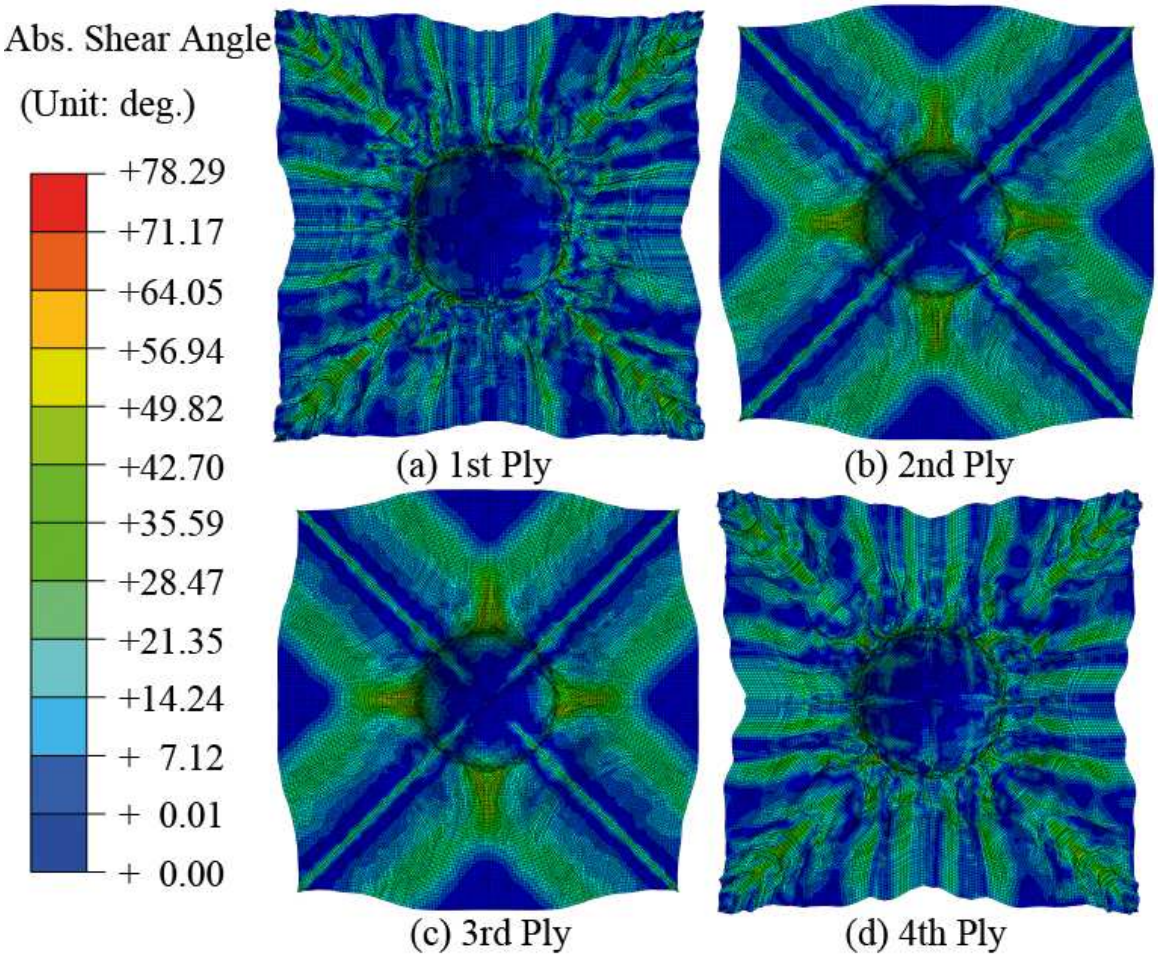

Fig. 6: Results of forming simulation for a [(0°/90°) / ±45°]s fabric stack with stitching from corner to corner along the two diagonals (maximum shear angle 78.29° in 4th ply).

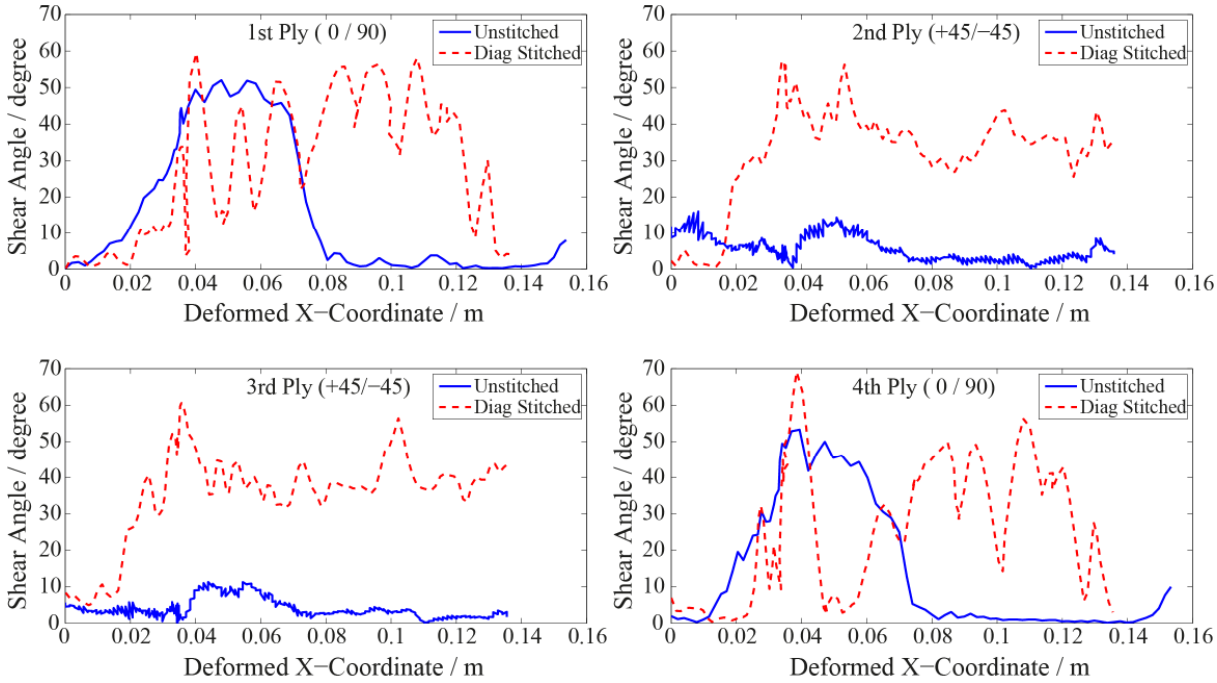

Fig. 7: Local shear angles plotted along a diagonal path from the centre of the hemisphere to the top-right corner (see Fig 6).

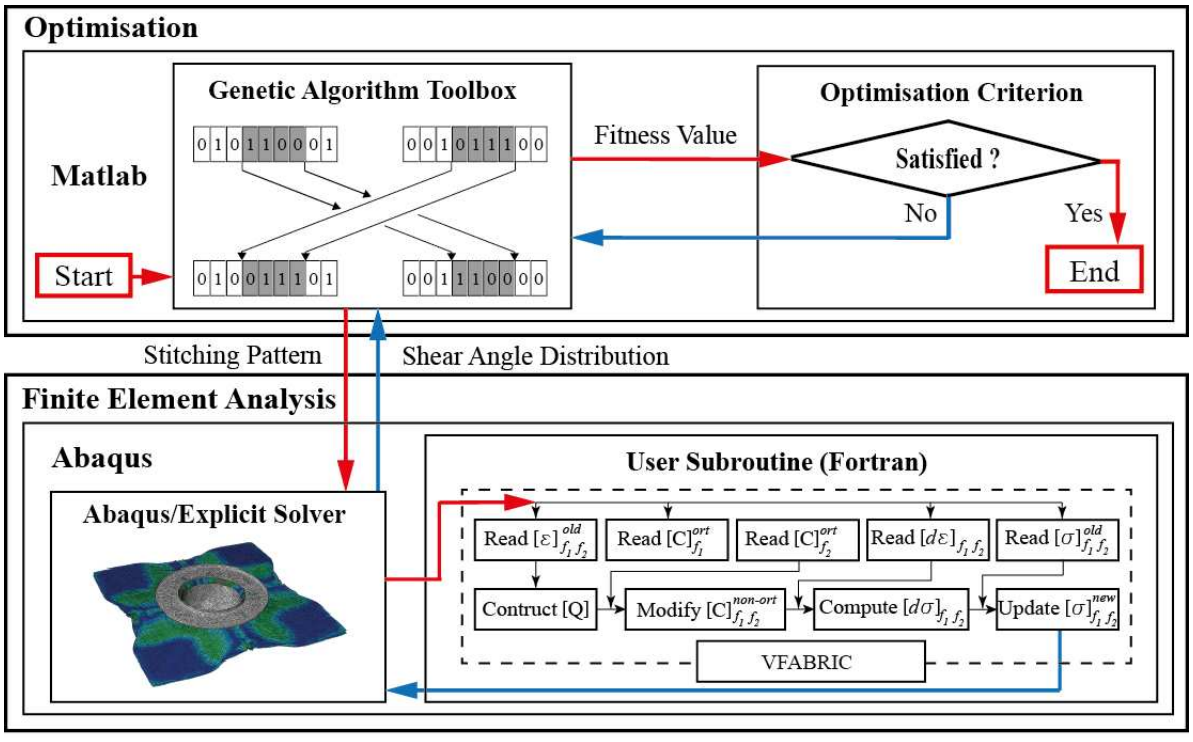

Fig. 8. Implementation of localised stitching optimisation.

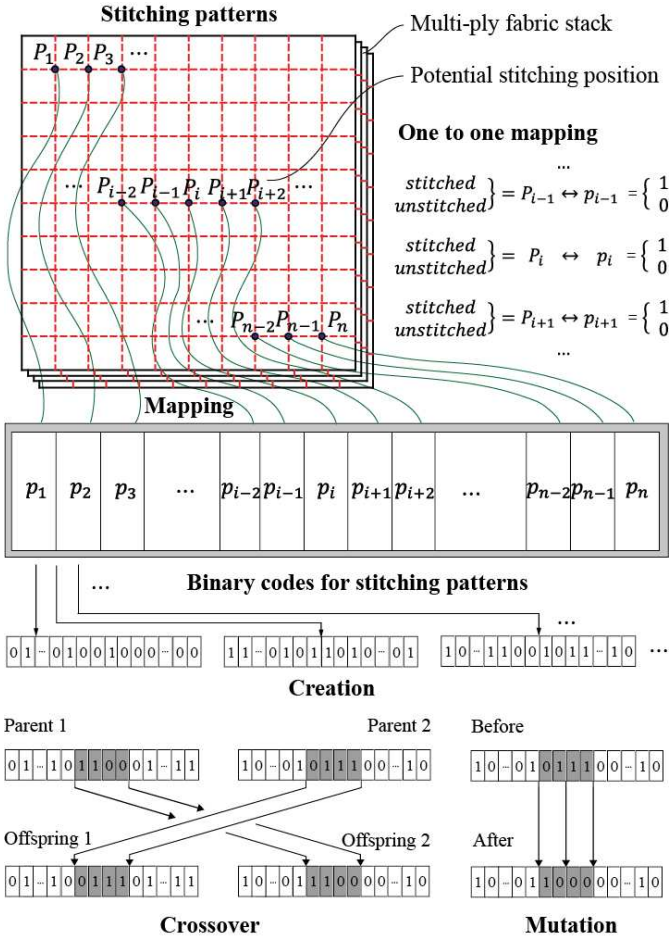

Fig. 9. Binary encoding and manipulation scheme for stitching pattern.

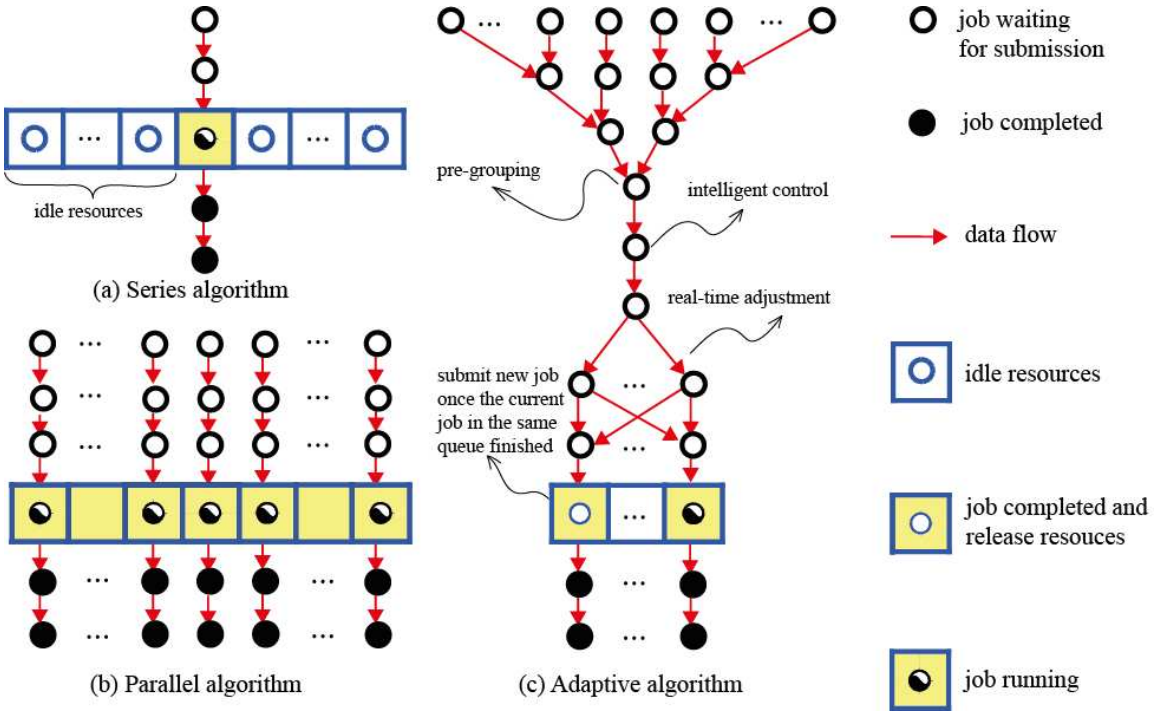

Fig. 10. Processing strategy for stitching optimisation.

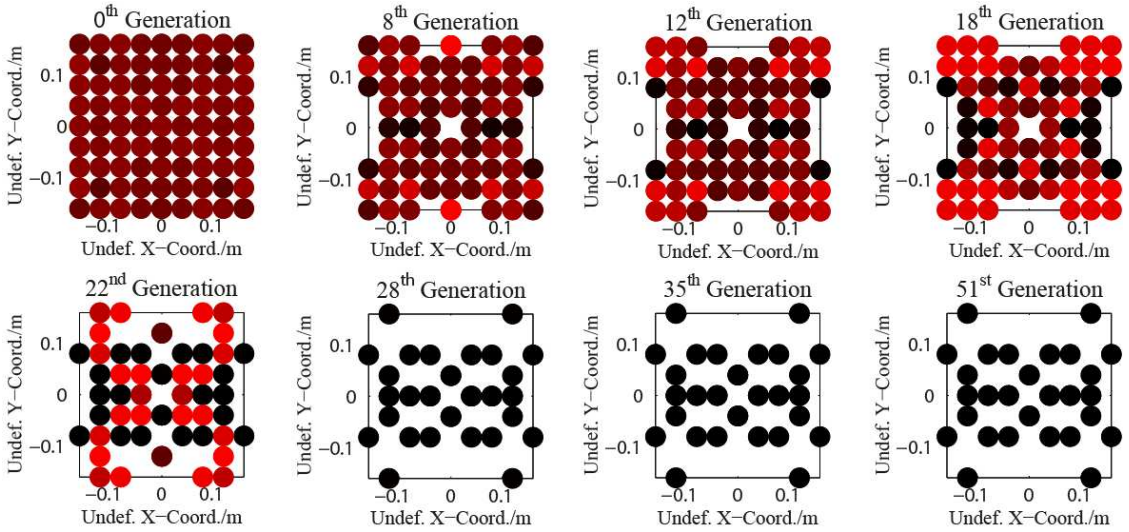

(a) Optimisation evolution of stitching pattern based on MAXVC.

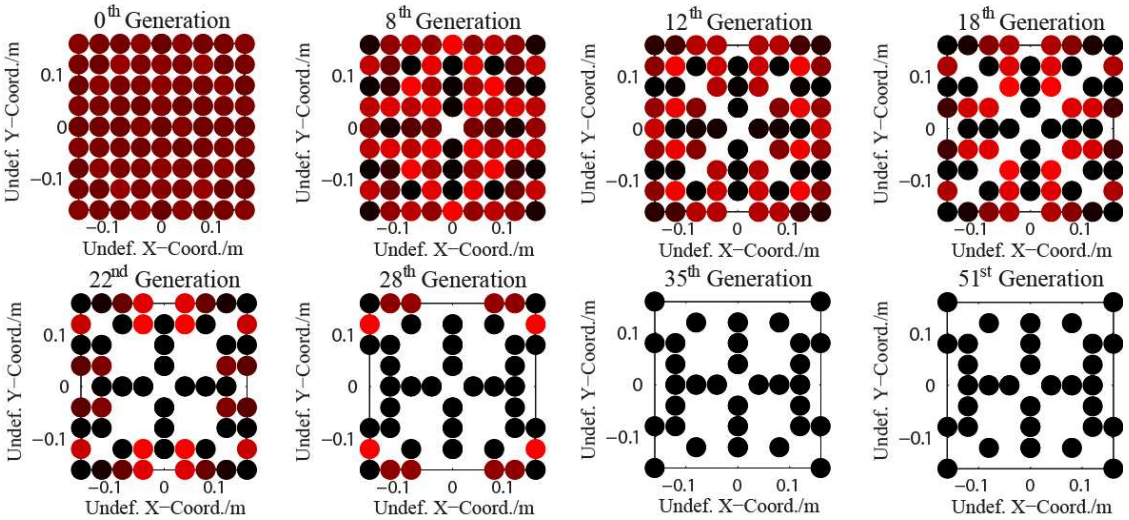

(b) Optimisation evolution of stitching pattern based on WBLQC.

Fig. 11. Optimisation evolution of stitching pattern based on MAXVC (Top) and WBLQC (Bottom). Solid points represent stitching positions in the respective generation; red scale indicates the frequencies of occurrence within the respective generation.

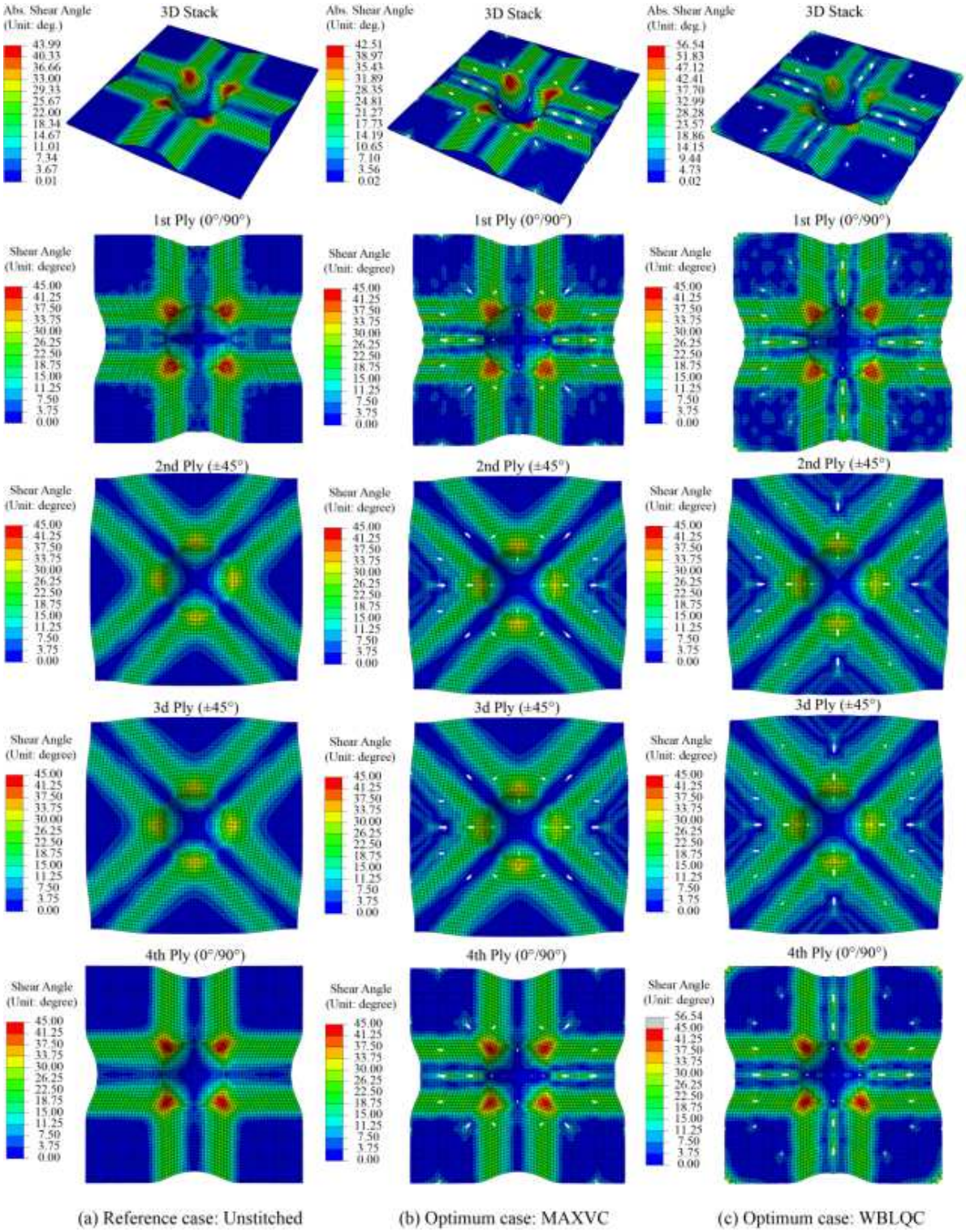

Fig. 12. Shear angles and deformed configurations of preform assembly from MAXVC and WBLQC criteria compared against unstitched reference case; white points represent stitching positions; the maximum shear angles are 43.99° (unstitched), 42.51° (MAXVC) and 56.54° (WBLQC).

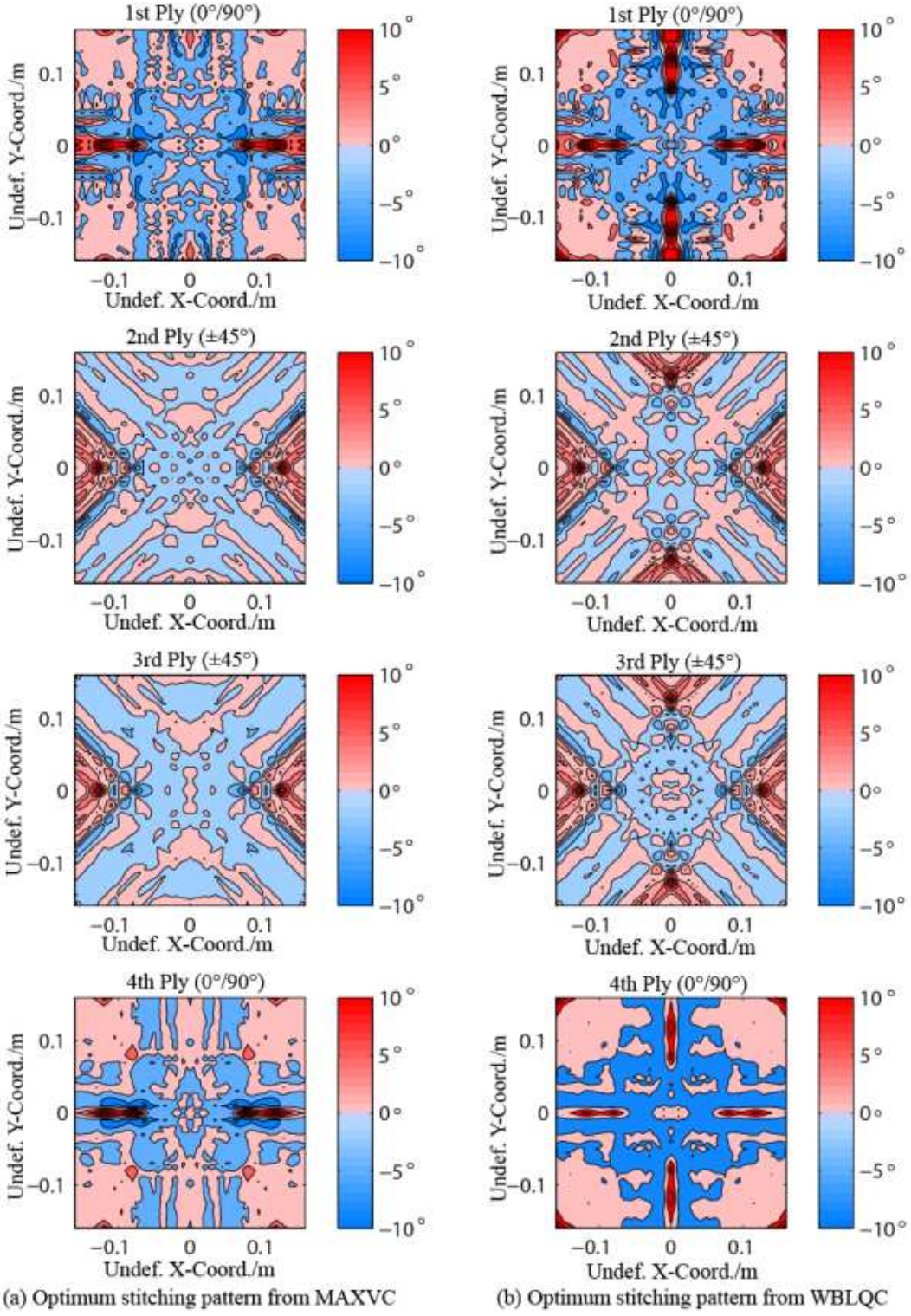

Fig. 13. Shear angle distributions normalised with respect to the unstitched case, plotted on the undeformed blank shape; (a) using MAXVC; (b) using WBLQC; shear angle distributions are; blue regions indicate reduced shear angles and red indicates increased shear angles over the unstitched case.

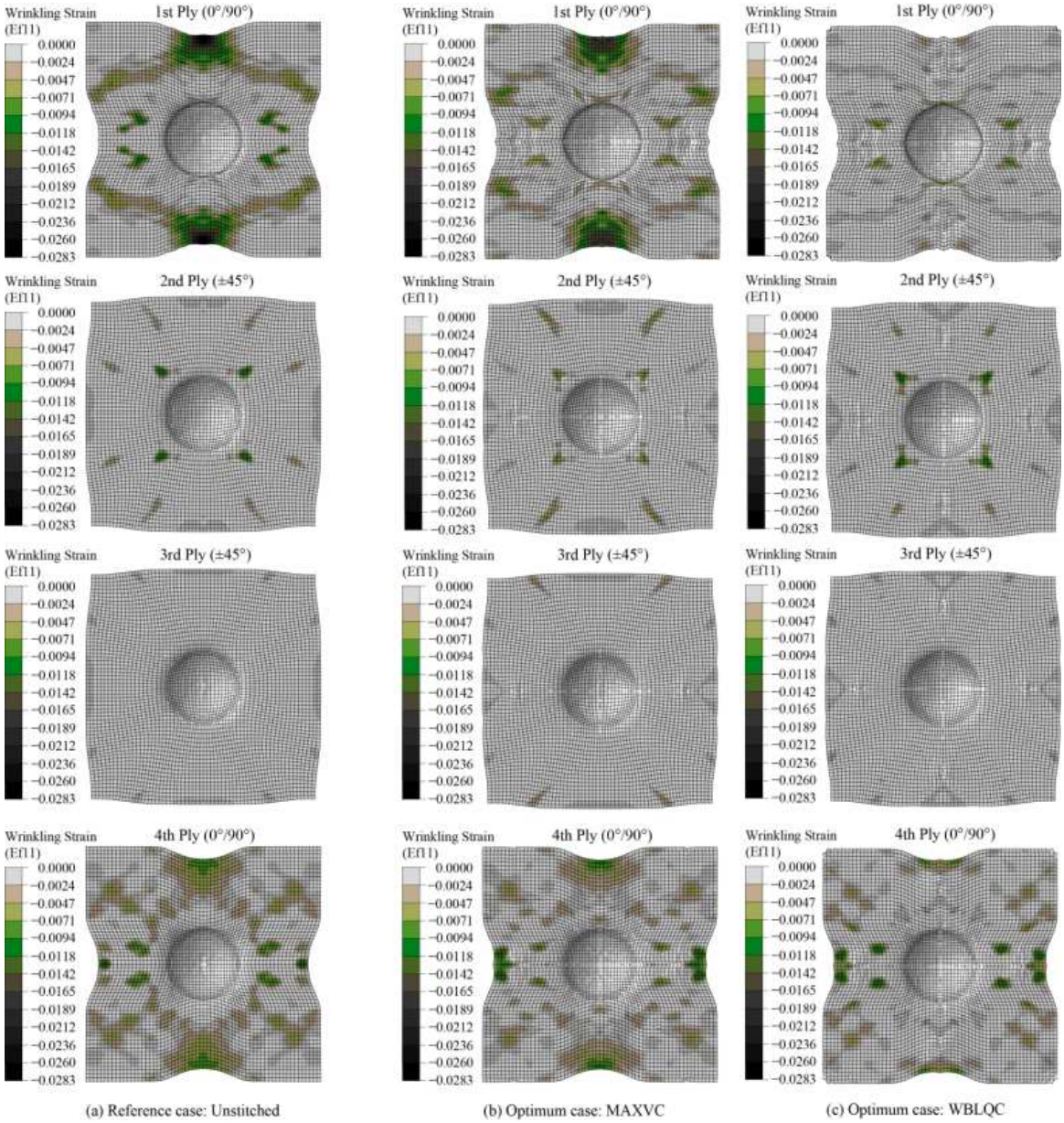

Fig. 14: Wrinkling strain along 1st fibre orientation.